

# A modelling analysis of human optic nerve fibres excitation based on experimental data

Simone Parrini <sup>(1)</sup>      Jean Delbeke <sup>(1)</sup>      Vincent Legat <sup>(2)</sup>  
Claude Veraart <sup>(1)</sup>

(1) Neural Rehabilitation Engineering Laboratory, and (2) CESAME Applied Mechanics, Université Catholique de Louvain, Belgium.

*Corresponding author:*

Prof. C.Veraart

Neural Rehabilitation Engineering Laboratory (GREN)

Avenue Hippocrate 54, box UCL 54.46

B 1200 Brussels, Belgium

*phone:* +32 2 7645446

*fax:* +32 2 7649422

*e-mail:* veraart@gren.ucl.ac.be

**Abstract:** This modelling study is based on experimental data concerning electrical stimulation of the human optic nerve in a blind volunteer (Veraart et al., 1998). First, we investigate whether the 2-channels mammalian myelinated fibre model proposed by Chiu et al. (1979), can be applied to the case of human optic nerve fibres. In order to answer this question, the macroscopic electric potential generated by an implanted cuff electrode is calculated using a 3D, inhomogeneous and anisotropic nerve model, taking into account possible variations of connective tissue thickness and neural tissue conductivity. Theoretical fibre excitation thresholds and conduction velocities are then calculated by assuming the 2-channels membrane description. Results show that the behaviour resulting from this 2-channels membrane model is not compatible with the experimental perception thresholds (Veraart et al., 1998) and with the conduction velocities measured in primates (Griffin & Burke, 1974). This is still true when the physical model parameters (ionic channel densities and passive cable parameters) are modified within a reasonable and physiological range. Finally, we show how the addition of a third slow-dynamics channel leads to a 3-channels model which adequately simulates the experimental data.

**Keywords:** Optic nerve, Spiral cuff electrode, Human, Fibre model, Ionic channels, Finite elements method, Bifurcations.

# 1 Introduction

Recently, electrical stimulation of the human optic nerve (ON) has been conducted using an implanted self-sizing spiral cuff electrode (Veraart et al., 1998). In the frame of these experiments, the development of a suitable model allowing the simulation of nerve fibres activation, would be undoubtedly useful.

The ON fibres, organised within a single cylindrical fascicle, are the myelinated axons of the retinal ganglion cells (RGC). Several studies provide evidences for the existence of three major RGC groups in the primates (see Stone, 1993, for a detailed review and discussion). The Y cells exhibit a transient response to steady illumination, and their receptive field centre-surround inhibitory mechanism involves non linear summation processes. The Y cells are related to spatial localisation, movement perception and black & white vision. The corresponding fibres have an average conduction velocity of  $22\text{ m/s}$  (Griffin & Burke, 1974); they have large diameter and represent a small percentage of the population. The X cells exhibit a sustained response to steady illumination, and their receptive field centre-surround inhibitory mechanism involves linear summation processes. The X cells are related to pattern-colour recognition. The corresponding fibres have an average conduction velocity of  $11\text{ m/s}$  (Griffin & Burke, 1974), medium-size

diameter and represent about half of the population. The remaining W-type cells, present slow-conducting and small-diameter fibres.

Globally, the electrical behaviour of a myelinated nerve fibre depends on the geometrical parameters and on the ionic channels at the nodes of Ranvier.

The available information about the primate ON fibres geometry (axon and fibre diameters, internodal length and active node length) is restricted to the fibre diameter spectrum: Jonas et al. (1990) report an average value of 1  $\mu m$ . It seems reasonable to expect that this mean value is representative of X-fibres population (Stone, 1993). These data, together with the conduction velocity values reported by Griffin and Burke (1974) are likely to provide an indirect information source for the estimation of the other geometrical parameters.

Concerning the membrane description at the nodes of Ranvier, the most popular model for mammalian applications is probably that proposed by Chiu et al. (1979). This model includes only voltage-regulated sodium currents, with no active potassium channels, membrane repolarisation being completely due to leakage currents. Chiu's model was validated on the rabbit sciatic nerve, and has been adopted in the frame of several modelling studies oriented to peripheral nerve applications (Chintalacharuvu et al., 1991; Rijkhoff et al., 1994; Goodall et al., 1995; Deurloo et al., 1998).

On the other hand, the only model for the retinal ganglion cell is that proposed by Fohlmeister et al. (1990) for the repetitive firing of salamander RGC. This space-clamp model, including six ionic channels (five non-linear and one leakage), is based on experimental data collected on the cell soma and not on the myelinated axonal part of the cell which forms the optic nerve. Moreover, it is not clear whether the species involved is a good animal model for human applications, the visual system being very species-dependent.

No model for the primate ON fibres is available, nor any study provides qualitative information about the ionic channels. Such experiments are clearly bounded by ethical and technical problems.

The purpose of this study is to determine, on the basis of simulations, the simplest model which adequately predicts the experimental observations on primate ON fibres (Veraart et al., 1998, Griffin & Burke, 1974).

In this frame, we firstly investigate the suitability of a generalised version of Chiu's 2-channels model. We compute the macroscopic electric potential generated by the implanted cuff electrode using a 3D, inhomogeneous and anisotropic nerve model, taking into account possible variations of uncertain parameters (encapsulation tissue thickness and neural tissue conductivity). Then we calculate theoretical fibre excitation thresholds and conduction velocity, by assuming the 2-channels membrane description and letting the

physical model parameters (ionic channels density and passive cable parameters) vary within a reasonable and physiological range. The simulation results are compared with the experimental perception thresholds given by Veraart et al. (1998) and the conduction velocities reported by Griffin and Burke (1974).

In the last part, the addition of a third slow-dynamics channel is considered and the behaviour of the resulting 3-channels model is again compared to the experimental data.

## **2 Methods**

### **2.1 Experimental data**

The experimental data provided by Veraart et al. (1998) consist in perception thresholds, i.e. the minimal pulse amplitude (given the pulse duration, the stimulation frequency and the number of pulses) which is necessary to elicit a phosphene. As expected, shorter pulses require stronger currents. Also, a higher number of pulses or a higher stimulation frequency lowers the perception threshold indicating central temporal integration (Delbeke et al., 1999).

Table I reports the perception thresholds for various pulse durations, for a 17-pulses train at 160  $Hz$ , which are the highest number of pulses and stimulation frequency reported by Veraart et al. (1998).

From these data it is possible to deduce upper bounds for fibre activation thresholds. Indeed, the stimulation period corresponding to 160  $Hz$  (about 6  $ms$ ) is much greater than the typical nerve membrane time constant (Grill & Mortimer, 1995). Therefore, the nerve fibres are activated by *each* pulse of the train. Moreover, the phosphenes elicited at threshold are usually coloured, and this suggests that at least some X-like fibres are activated (Stone, 1993). It can thus be stated that some X-fibres exist in the nerve, whose strength-duration curves (Mortimer, 1990) do not lie above the points of Table I.

Concerning the conduction velocity, we refer to data published by Griffin and Burke (1974) and discussed by Stone (1993) which show the existence, in the primate, of a X-like cell group having a velocity of 11  $m/s$ .

The threshold current that has to be injected through an electrode contact in order to excite a given nerve fibre depends on the electric field distribution within the nerve (thus, on tissue dimensions and conductivity values), and also on the microscopic parameters describing the fibre behaviour. On the other hand, the conduction velocity is only determined by the microscopic fibre description.

## 2.2 The volume conductor model

The whole domain is a cylinder (radius 6 *mm*, length 16 *mm*) as shown in Figure 1. The fibres fascicle is modelled as a cylinder of 2.7 *mm* diameter, as measured in the volunteer by magnetic resonance imaging. The fascicle is surrounded by a layer of connective tissue (conductivity: 0.0659 *S/m*, from Chintalacharuvu et al., 1991). The implanted cuff is 0.25 *mm* thick and 6.6 *mm* long with four recessed disk contacts at four angular positions in the transverse plane, as shown in the figure; these contacts are modelled as equivalent squares (contact thickness 0.025 *mm*, square contact side 0.9 *mm*, square window side 0.45 *mm*, recess 0.08 *mm*). The nerve and the cuff are considered immersed in saline (conductivity: 2 *S/m*, from Geddes & Baker, 1967).

Data from the literature about the thickness of the connective tissue layer developed by the nerve as a response to the implant, concern either cuff electrodes implanted around the peripheral nerve (Grill & Mortimer, 1994), or flat electrodes implanted on the cortex (Brindley & Levin, 1968, reported a connective tissue layer of about 80  $\mu\text{m}$ ). Indeed, the biological response of the Central Nervous System to an implanted body is, in general different to that of peripheral nerves. This is the reason why, in our model, we consider two extreme cases: no encapsulation tissue (zero thickness layer) or a 100



$\mu m$  connective layer.

The nerve fascicle conductivity is also somewhat uncertain: within the previously published modelling studies, some authors consider 0.1  $S/m$  transversely and 1  $S/m$  longitudinally (eg. Chintalacharuvu et al., 1991), while others consider 0.08 and 0.5 1  $S/m$  (eg. Goodall et al., 1995). We consider both situations in our model. Possible variations in connective tissue thickness and nerve conductivity will be taken into account, by defining the four situations summarised in Table II.

In each case, we evaluate the electric potential distribution by solving Poisson's equation in the domain. The numerical technique is a mixed Finite Elements - Fourier approach which allows the calculation of the 3D solution at low cost, as described by Parrini et al. (1999).

### 2.3 The fibre cable equation

Assuming that myelin is a perfect insulator and that the active node length is much smaller than the internodal one, the myelinated fibre can be described by an equivalent circuit (McNeal, 1976), whose mathematical description is:

$$\frac{dv_j}{dt} = -\frac{1}{c}i_j^{ionic} + \frac{d}{4c\rho lL}\Delta_2(v_j + v_j^{ext}) \quad (1)$$

at each node  $j$ , where:

- $t$  is the time ( $ms$ )

- $v_j^{ext}$  is the extracellular potential ( $mV$ ) at node  $j$ ; its value is known from the volume conductor part, thus is affected by the macroscopic parameters;  $v_j^{ext}$  also depends from the internodal length;
- $v_j$  is the transmembrane potential ( $mV$ ) and is a function of time ( $v_j(0) = 0$ );
- $\Delta_2 x_j \doteq x_{j-1} - 2x_j + x_{j+1}$ ;
- the passive cable parameters  $c$ ,  $d$ ,  $\rho$ ,  $l$ ,  $L$  are respectively the membrane capacitance ( $\mu F cm^{-2}$ ), the axon diameter ( $cm$ ), the axoplasm resistivity ( $k\Omega cm$ ), the active node length and the internodal distance ( $cm$ ).

No direct hystological data are available in the literature about the geometrical cable parameters  $l$ ,  $d$  and  $L$  of the human ON. Jonas et al. (1990) give detailed information about the *fibre* diameter ( $D$ ) spectrum, showing a distribution mean of  $1 \mu m$ , that we consider representative of the X-fibres population considered in this study (Stone, 1993). On the basis of this value, we have to estimate *reasonable ranges of variation* for  $l$ ,  $d$  and  $L$ , using relationships which have been observed in the peripheral nerve and have been adopted by the related modelling studies. The axon diameter is usually considered as  $d = 0.6D$  (eg. Goodall et al., 1995) or  $d = 0.7D$  (McNeal, 1976);

so, setting  $D = 10^{-4} \text{ cm}$ , we consider  $d$  varying between  $0.6 \cdot 10^{-4}$  and  $0.7 \cdot 10^{-4} \text{ cm}$ . The internodal distance is taken as  $L = 100D$  by all the previously cited authors, whereas data reported by Butt and Jenkins (1994) on the mouse optic nerve suggest  $L = 200D$ ; thus we let  $L$  vary between  $0.01$  and  $0.02 \text{ cm}$ . The active node length is always set to  $1.5 \mu\text{m}$  whatever the fibre diameter, in the peripheral nerve case; however, since optic nerve fibres are (more than 10 times) thinner than peripheral ones, one can expect a lower value: we adopt  $1.5 \cdot 10^{-4} \text{ cm}$  as the upper bound and  $0.5 \cdot 10^{-4} \text{ cm}$  as the lower bound for the  $l$  variation range.

Concerning the electrical cable parameters  $c$  and  $\rho$ , they should not differ according to the nerve, but one can find different values in the literature, so in practice we adopt a range of variation for them, too. Table III summarises the range of variation considered here for all the cable parameters.

These parameters do not contribute independently to the equations. We define the ratio:

$$r = \frac{d}{4c\rho l} \quad (2)$$

From the previous table and (2), it follows that  $r$  varies between  $0.36$  and  $3.5 \text{ cm/ms}$ . Clearly, the conduction velocity depends on  $r$ ,  $L$  and  $i^{ionic}/c$ . Also the excitation threshold depends on these parameters, plus of course those

of the volume conductor and the fibre location.

## 2.4 The 2-channels membrane model

Chiu's description for ionic currents, adapted by Sweeney et al. (1987) to the temperature of 37 degrees, includes voltage-regulated sodium channels and passive leakage ones. At node  $j$ :

$$i_j^{ionic} = \hat{g}_{Na} m_j^2 h_j (v_j - E_{Na}) + \hat{g}_L (v_j - E_L) \quad (3)$$

$$\frac{dm_j}{dt} = \underbrace{\frac{0.363v_j + 96.96}{1 + \exp\left(\frac{-v_j + 31}{5.3}\right)}}_{\alpha_m(v_j)} (1 - m_j) - \underbrace{\alpha_m(v_j) \exp\left(\frac{23.8 - v_j}{4.17}\right)}_{\beta_m(v_j)} m_j \quad (4)$$

$$\frac{dh_j}{dt} = \underbrace{\beta_h(v_j) \exp\left(\frac{5.5 - v_j}{5}\right)}_{\alpha_h(v_j)} (1 - h_j) - \underbrace{\frac{15.6}{1 + \exp\left(\frac{-v_j + 24}{10}\right)}}_{\beta_h(v_j)} h_j \quad (5)$$

where  $E_{Na} = 115.64 \text{ mV}$  (sodium resting potential) and  $E_L = -0.011 \text{ mV}$  (leakage resting potential). The initial conditions are  $m_j(0) = 0.0033$  and  $h_j(0) = 0.7503$ . The parameters  $\hat{g}_{Na}$  and  $\hat{g}_L$  are related to membrane channel density; their original values are  $\hat{g}_{Na} = 1445 \text{ k}\Omega^{-1} \text{ cm}^{-2}$  and  $\hat{g}_L = 128 \text{ k}\Omega^{-1} \text{ cm}^{-2}$ . We denote this model, as the CS model. In what follows, we will also consider a generalised version of the CS model, in which the channels density parameters  $\hat{g}_{Na}$  and  $\hat{g}_L$  are varied. This generalised CS model will be called the 2-channels model.

## 2.5 Implementation and simulation strategy

The volume conductor and the fibre models are implemented in a computer software. Given the volume conductor parameters, the electric potential within the whole nerve is computed (Parrini et al., 1999). Then, given the fibre position within the nerve and the internodal length  $L$ , the extracellular potential  $v_j^{ext}$  is extracted at the nodes of Ranvier and the ordinary differential equations system (1) for a given choice of  $r$  and ionic current description, is solved by a 4-5th order Runge-kutta adaptive scheme. The fibre is defined as excited if the transmembrane potential at the last node of Ranvier (at the domain boundary) reaches 80  $mV$ . The conduction velocity is evaluated on the basis of the time interval between the action potential peaks of two adjacent nodes of Ranvier.

As a first attempt, we adopt the CS ionic current description and try to reach the desired results (thresholds and conduction velocity) by only changing the passive cable parameters  $r$  and  $L$ .

In a second approach, we consider the 2-channels model (generalised CS model), where the four parameters  $r$ ,  $L$ ,  $\hat{g}_{Na}/c$  and  $\hat{g}_L/c$  are varied simultaneously in order to minimise the distance between the model response and the target one. For this, we use a standard Simplex search algorithm implemented in the MATLAB<sup>TM</sup> optimisation toolbox. The distance is defined

as follows:

$$distance = \sqrt{\left(\frac{thr - thr_0}{thr_0}\right)^2 + \left(\frac{vel - vel_0}{vel_0}\right)^2} \quad (6)$$

where  $(thr, vel)$  are respectively the predicted threshold for a 0.1 *ms* pulse duration and the predicted conduction velocity;  $(thr_0, vel_0)$  are the desired values: 0.055 *mA* and 11 *m/s*. For each value of  $\hat{g}_{Na}/c$  and  $\hat{g}_L/c$ , the leakage resting potential  $E_L$  is evaluated so that the total ionic current given in (3) is zero at  $t = 0$ .

When modifying the ionic channels density, we may change the stability properties of the system itself. In order to illustrate how these properties may change, we use the space-clamped system (Grill & Mortimer, 1995), i.e. a reduced system where only one node of Ranvier is described (no propagation is considered). This system respects the qualitative behaviour of the full model and allows simulations at a lower cost.

Finally, we will consider the addition of a third channel (3-channels model) and analyse the consequent model response.

## 3 Results

### 3.1 Effect of the volume conductor parameters

Figure 2 shows the excitation threshold (for a 0.1 *ms* pulse duration) in the four cases  $C_0K_{0.1-1}$ ,  $C_0K_{0.08-0.5}$ ,  $C_{100}K_{0.1-1}$  and  $C_{100}K_{0.08-0.5}$ , as defined in Table II. The fibre is assumed to be parallel to the nerve axis, with a node of Ranvier on the transverse symmetry plane (most favourable case); three fibre positions are considered: at the fascicle surface, under the contact (depth=0); at the fascicle centre (depth=1); at the middle point (depth=0.5). In all cases the CS ionic current description is assumed, with  $L = 0.02$  *cm* and  $r = 0.5714$  *cm/ms* ( $d = 0.6 \cdot 10^{-4}$  *cm*,  $l = 1.5 \cdot 10^{-4}$  *cm*,  $c = 2$   $\mu F/cm^2$ ,  $\rho = 0.07$   $k\Omega cm$ ).

We observe that the  $*K_{0.08-0.5}$  cases present lower thresholds than the  $*K_{0.1-1}$  ones; moreover, the presence of the connective tissue ( $C_{100}$  cases) increases the threshold of the superficial fibre (as expected) but lowers that of the central one (i.e. connective tissue allows a more uniform current distribution within the nerve). Although the threshold values calculated here clearly depend on the fibre model, the relative positions of the curves in Figure 2 is only determined by the current penetration within the nerve, i.e. by the volume conductor parameters. Therefore, the qualitative considerations exposed above are valid whatever the fibre model.

In what follows, we retain the “best case”, i.e. the  $C_0K_{0.08-0.5}$  situation which gives the lowest threshold (0.19 mA) for a superficial fibre. Note that even in this case, the threshold value obtained with standard fibre parameters is about 4 times greater than the desired one (0.055 mA). The conduction velocity predicted with these values is about 6 m/s in all the situations.

### 3.2 Response of the CS model with varying cable parameters

Considering a superficial fibre in the  $C_0K_{0.08-0.5}$  situation and assuming the CS ionic current description, we compute the conduction velocity and the excitation threshold for a 0.1 ms pulse duration, when  $L$  varies between 0.01 and 0.02 cm and  $r$  varies between 0.36 and 3.5 cm/ms. The results are illustrated in Figure 3.

The lowest threshold (0.08 mA) is obtained for  $L = 0.02$  cm and  $r \geq 2.5$  cm/ms), but the corresponding velocity is above 15 m/s. Threshold calculation for other pulse durations with  $L = 0.02$  cm and  $r = 3$  cm/ms, shows that the resulting strength-duration curve is definitely not compatible with the experimental results (Figure 4).

### 3.3 Response of the generalised 2-channels model

We now let all the parameters  $\hat{g}_{Na}/c$ ,  $\hat{g}_L/c$ ,  $r$ ,  $L$  vary according to the optimisation algorithm. Considering  $c = 2.5 \mu F/cm^{-2}$  and the CS values for



the ionic channel densities, the starting values for  $\hat{g}_{Na}/c$  and  $\hat{g}_L/c$  are respectively 578 and  $51.2 \text{ ms}^{-1}$ . In searching the optimum answer, the algorithm monotonously increases the former and decreases the latter. For:

$$\frac{\hat{g}_{Na}}{c} = 1064 \text{ ms}^{-1}, \frac{\hat{g}_L}{c} = 4.17 \text{ ms}^{-1}, r = 0.4601 \text{ cm/ms}, L = 0.02 \text{ cm} \quad (7)$$

the threshold is  $0.057 \text{ mA}$  and the velocity is  $10.7 \text{ m/s}$ . This seems satisfactory, but such big changes in the original channel parameters make us wonder whether the system stability characteristics are preserved.

Figure 5 shows a threshold simulation in the 2-channels space-clamped system, when the ionic channel densities are set as in (7): a second equilibrium point ( $v \approx 36 \text{ mV}$ ,  $m \approx 0.9$ ,  $h \approx 0$ ) appears beside the resting state. The solution is attracted by this point with damped oscillations. Such behaviour is clearly unphysiological: by modifying the original CS values, we have denatured the system itself, which has undergone a bifurcation.

Figure 6a illustrates the equilibria  $v_{eq}$  of the  $v$  variable as a function of  $\hat{g}_L/c$ , when  $\hat{g}_{Na}/c$  is kept fixed to its original value: the point  $(\hat{g}_L/c)_0 \approx 13 \text{ ms}^{-1}$  is a bifurcation point, because for  $\hat{g}_L/c > (\hat{g}_L/c)_0$  the system has only one equilibrium point (the resting state), but for  $\hat{g}_L/c < (\hat{g}_L/c)_0$  there are two additional equilibria.

The stability and the nature of these equilibria is determined by the jacobian of the system evaluated at the equilibrium itself.

In our case, we must determine the physiological region of the plane  $(\hat{g}_{Na}/c, \hat{g}_L/c)$ , i.e the values of the channel densities which give only one equilibrium point. This region is illustrated in Figure 6b.

When we constrain the parameters to vary within this region, the lowest threshold which can be obtained for a 0.1 *ms* pulse, is 0.065 *mA*, corresponding to a conduction velocity of 16 *m/s*.

In conclusion, the 2-channel model cannot simulate the experimental observations.

### 3.4 Addition of a third slow-dynamics channel

Setting the parameters as in (7) resulted in good short-time responses (threshold and conduction velocity) but bad long-time behaviour (oscillations and a bad final state). The addition of a slow variable may fix the equilibrium problem, still keeping the threshold and velocity unchanged.

The slow variable  $n$  describing the potassium channels, presented by Hodgkin and Huxley (1952), may be suitable.

We consider a 3-channel ionic currents description as follows:

$$\frac{i_j^{ionic}}{c} = \frac{\hat{g}_{Na}}{c} m_j^2 h_j (v_j - E_{Na}) + \frac{\hat{g}_L}{c} (v_j - E_L) + \frac{\hat{g}_K}{c} n_j^4 (v_j - E_K) \quad (8)$$

where  $\hat{g}_{Na}/c = 1064 \text{ ms}^{-1}$ ,  $\hat{g}_L/c = 4.17 \text{ ms}^{-1}$  as in equation (7), and  $E_K = -12 \text{ mV}$  (from Hodgkin & Huxley, 1952). The  $n$  variable is governed

by an equation analogous to (4) with the rate constants defined as:  $\alpha_n(v) = \alpha_m(v)/20$ ,  $\beta_n(v) = \beta_m(v)/60$ . This is a rough imitation of the Hodgkin and Huxley's model.

Clearly, for  $\hat{g}_K/c = 0 \text{ ms}^{-1}$  the model reduces to the 2-channels one, thus exhibiting the unphysiological behaviour. Figure 7 illustrates the equilibria  $v_{eq}$  of the  $v$  variable, in the space-clamped system, as a function of  $\hat{g}_K/c$ , when  $\hat{g}_{Na}/c$  and  $\hat{g}_L/c$  are kept fixed. For  $\hat{g}_K/c < (\hat{g}_K/c)_0 \approx 1840 \text{ ms}^{-1}$ , the system presents the unphysiological 3 equilibria; for  $\hat{g}_K/c > (\hat{g}_K/c)_0$  only one equilibrium point (the resting state) is present.

Thus, the third channel can restore the right behaviour provided that  $\hat{g}_K/c > 1840 \text{ ms}^{-1}$ . Figure 8 shows the response of the space-clamped system with  $\hat{g}_K/c = 1850 \text{ ms}^{-1}$ .

The complete system (with  $L = 0.02 \text{ cm}$  and  $r = 0.4601 \text{ cm/ms}$ ) predicts a threshold of  $0.057 \text{ mA}$  for a  $0.1 \text{ ms}$  duration and a conduction velocity of  $10.7 \text{ m/s}$ , whatever the value of  $\hat{g}_K/c$ . Indeed the short-time responses (threshold and conduction velocity) are independent of the third slow channel density (results not shown) .

The calculation of the activation thresholds for other pulse durations, on the basis of this 3-channels model with  $\hat{g}_K/c = 1850 \text{ ms}^{-1}$  , leads to a strength-duration curve (Figure 9), which is clearly consistent with the

experimental data.

## 4 Discussion

The results demonstrate that the 2-channels membrane model proposed by Chiu et al. (1979) cannot be applied to human optic nerve fibres, because the obtained behaviour is not compatible with the human perception thresholds reported by Veraart et al. (1998) and the conduction velocities measured in primates (Griffin & Burke, 1974), even when the physical model parameters (ionic channel densities and passive cable parameters) are modified within a reasonable and physiological range.

This conclusion is based on two assumptions. The first one is that the monkey is a suitable animal model, so that the conduction velocity of X-like human optic nerve fibres is about 11  $m/s$ . Actually, as far as the velocity is lower than 16  $m/s$ , the results are unchanged (see section 3.3). The second assumption is that human colour-coding fibres are comparable to those of the other primates (Stone, 1993) and thus contribute to the 1  $\mu m$  peak value of fibre diameter (Jonas et al., 1990).

Clearly, the construction of an adequate mathematical model needs an experimental support: not only the action potential shape to be reproduced must be known, but if one desires a physical (and not a “black box”) model,

also the specific ionic channels must be identified and their physical properties measured. Technical problems related to voltage and/or patch clamp of such small-diameter fibres are a major issue.

On the other hand, the definition of a simple model reproducing all the experimental data available up to date is very useful to allow for simulation studies in the frame of human experiments. We have shown that, provided a new channel is postulated in the fibre membrane, it is possible to obtain the desired model behaviour. Since many studies demonstrate the existence of potassium channels in rat ON fibres (Gordon et al., 1988), the new channel was inspired by the  $K^+$  channel model presented by Hodgkin and Huxley (1952), with slight modifications.

The fact that this 3-channels model adequately simulates the experimental observations, must not be taken as an evidence that potassium channels actually take part to the excitation process in human ON fibres, nor that sodium and potassium are the only active channels. Indeed, the fact that we doubled the sodium channels density with respect to the peripheral nerve case, could suggest that a second fast ion species (eg. calcium, see Sun & Chiu, 1999) could be present and thus “double” the sodium effect. These points can be established only experimentally. We hope that this study can stimulate experimental research in order to assess membrane properties in

primates optic nerve fibres.

**Acknowledgements** - We are indebted to Prof. J-M.Lebacq and Dr. Ph.Gailly for a critical reading of the manuscript. This work was supported by the Commission of the European Union (MIVIP project, ESPRIT LTR 22 527 and SENSATIONS project, BIOMED BMH4-CT-96-0897) and by the Belgian F.M.S.R. (grant 3.4584.98).

## References

- Brindley, G., & Levin, W. (1968). The sensations produced by electrical stimulation of the visual cortex. *J.Physiol.*, 196, 479-493.
- Butt, A., & Jenkins, H. (1994). Morphological changes in oligodendrocytes in the intact mouse optic nerve following intravitreal injection of tumour necrosis factor. *J.Neuroimmunol.*, 51(1), 27-33.
- Chintalacharuvu, R., Ksienski, D., & Mortimer, J. (1991). A numerical analysis of the electric field generated by a nerve cuff electrode. *Proc. of the IEEE-Eng. Med. Biol. Soc. 13th Ann. Conf.*, 13(2), 912-913.
- Chiu, S., Ritchie, J., Rogart, R., & Stagg, D. (1979). A quantitative description of membrane currents in rabbit myelinated nerve. *J.Physiol.*, 292, 149-166.
- Delbeke, J., Parrini, S., Glineur, O., Vanlierde, A., & Veraart, C. (1999). Phosphene perception thresholds to direct stimulation of a human optic nerve shows spatial and temporal summation. *Soc. for Neurosci. Abstracts*, 25, 1042.
- Deurloo, K., Holsheimer, J., & Boom, H. (1998). Transverse tripolar stimu-



- lation of peripheral nerve: a modelling study of spatial selectivity. *Med. Biol. Eng. Comput.*, 36, 66-74.
- Fohlmeister, J., Coleman, P., & Miller, R. (1990). Modeling the repetitive firing of retinal ganglion cell. *Brain Res.*, 510, 343-345.
- Geddes, L., & Baker, L. (1967). The specific resistance of biological material - a compendium of data for the biological engineer and physiologist. *Med. Biol. Eng.*, 5, 271-293.
- Goodall, E., Kosterman, L., & Struijk, J. (1995). Modeling study of activation and propagation delays during stimulation of peripheral nerve fibers with a tripolar cuff electrode. *IEEE Trans. Rehab. Eng.*, 3(3), 272-282.
- Gordon, T., Kocsis, J., & Waxman, S. (1988). Evidence for the presence of two types of potassium channels in the rat optic nerve. *Brain Res.*, 477(1), 1-9.
- Griffin, A., & Burke, W. (1974). The distribution and nerve fibre groups in the optic tract and lateral geniculate nucleus of macaca irus. *Proc. Aust. Physiol. Pharmacol. Soc.*, 5, 74P.
- Grill, W., & Mortimer, J. (1994). Electrical properties of implant encapsulation tissue. *Ann. of Biomed. Eng.*, 22, 23-33.

- Grill, W., & Mortimer, J. (1995). Stimulus waveforms for selective neural stimulation. *IEEE-Eng. Med. Biol. Soc. magazine, July-August*, 375-385.
- Hodgkin, A., & Huxley, A. (1952). A quantitative description of membrane current and its application to conduction and excitation in nerve. *J.Physiol.*, 117, 500-544.
- Jonas, J., Muller-Bergh, J., Schlotzer-Schrehardt, U., & Naumann, G. (1990). Histomorphometry of the human optic nerve. *Invest. Ophthalmol. Visual Sc.*, 31(4), 736-744.
- McNeal, D. (1976). Analysis of a model for excitation of myelinated nerve. *IEEE Trans. Biomed. Eng.*, 23, 329-337.
- Mortimer, J. (1990). Electrical excitation of nerve. In A. W.F. & D. McCreery (Eds.), *Neural prostheses: fundamental studies* (p. 81-82). Englewood Cliffs: Prentice Hall.
- Parrini, S., Romero, E., Delbeke, J., Legat, V., & Veraart, C. (1999). A hybrid finite elements- spectral method for computation of the electric potential generated by a nerve cuff electrode. *Med. Biol. Eng. Comput.*, 37, in press.

- Rijkhoff, N., Holsheimer, J., Koldewijn, E., Struijk, J., Kerrebroek, P. V., Debruyne, F., & Wijkstra, H. (1994). Selective stimulation of sacral roots for bladder control: a study by computer modeling. *IEEE Trans. Biomed. Eng.*, *41*, 413-424.
- Stone, J. (1993). *Parallel processing in the visual system*. New York: Plenum Press.
- Sun, B., & Chiu, S. (1999). N-type calcium channels and their regulation by gabab receptors in axons of neonatal rat optic nerve. *J. Neurosci.*, *19*, 5185-5194.
- Sweeney, J., Mortimer, J., & Durand, D. (1987). Modeling of mammalian myelinated nerve for functional neuromuscular stimulation. *Proc. of the IEEE-EMBS 9th Ann. Conf.*, 1577-1578.
- Veraart, C., Raftopoulos, C., Mortimer, J., Delbeke, J., Pins, D., Michaux, G., Vanlierde, A., Parrini, S., & Wanet-Defalque, M.-C. (1998). Visual sensations produced by optic nerve stimulation using an implanted self-sizing spiral cuff electrode. *Brain Res.*, *813*, 181-186.
- Warman, E., Grill, W., & Durand, D. (1992). Modeling the effects of electric fields on nerve fibers: determination of excitation thresholds. *IEEE Trans. Biomed. Eng.*, *39*, 1244-1254.

pulse width ( <i>ms</i> )	threshold ( <i>mA</i> )
0.025	0.286
0.05	0.100
0.1	0.055
0.2	0.040
0.4	0.034

Table I: Perception thresholds for various pulse durations (17 pulses at 160 *Hz*). Data from (Veraart et al., 1998).

case	conn.tissue thickness ( $\mu m$ )	nerve conduct. (transv.-longitud. $S/m$ )
$C_0 K_{0.1-1}$	0	0.1-1
$C_0 K_{0.08-0.5}$	0	0.08-0.5
$C_{100} K_{0.1-1}$	100	0.1-1
$C_{100} K_{0.08-0.5}$	100	0.08-0.5

Table II: Four cases are defined in order to take into account possible variations in connective tissue thickness and nerve conductivity

parameter	unit	min	source	max	source
$c$	$\mu F cm^{-2}$	2	Goodall et al. (1995) Rijkhoff et al. (1994)	2.5	Warman et al. (1992)
$\rho$	$k\Omega cm$	0.05	Warman et al. (1992)	0.11	McNeal (1976)
$d$	$cm$	$0.6 \cdot 10^{-4}$	Warman et al. (1992) Goodall et al. (1995)	$0.7 \cdot 10^{-4}$	McNeal (1976)
$l$	$cm$	$0.5 \cdot 10^{-4}$	speculation	$1.5 \cdot 10^{-4}$	Goodall et al. (1995)
$L$	$cm$	0.01	McNeal (1976) Warman et al. (1992) Goodall et al. (1995)	0.02	Butt and Jenkins (1994)

Table III: Estimated variation ranges for the cable parameters.

## List of figure captions

**Figure 1** - Transverse (left) and longitudinal (right) sections of the volume conductor domain and its subdomains. The drawing is not to scale. See text for geometrical and electrical parameters.

**Figure 2** - Effect of the volume conductor parameters (see Table II) on the fibre threshold. The CS model is adopted with  $L = 0.02 \text{ cm}$  and  $r = 0.5714 \text{ cm/ms}$ . The vertical axis is log-scaled. The fibre depth (horizontal axis) is defined as the distance of the fibre from the fascicle surface divided by the fascicle radius.

**Figure 3** - Effect of  $r$  and  $L$  on the conduction velocity and the excitation threshold. In the right graph, the same graphic conventions as in the left one are adopted for the  $L$  values.

**Figure 4** - Threshold values for various pulse duration as predicted by the CS model (circles: 'o'), with  $r = 3 \text{ cm/ms}$  and  $L = 0.02 \text{ cm}$ . The continuous line shows Hill's interpolation (Mortimer, 1990) of these data, giving the strength-duration curve. The experimental data of Table I are also plotted (asterisks: '\*') for comparison purposes.

**Figure 5** - A threshold simulation in the 2-channels space-clamped system, when the ionic channel densities are set as in (7): a second equilibrium point ( $v_{eq} \approx 36 \text{ mV}$ ,  $m_{eq} \approx 0.9$ ,  $h_{eq} \approx 0$ ) appears beside the resting state.

**Figure 6** - Left: the equilibria of the  $v$  variable as a function of  $\hat{g}_L/c$ , when  $\hat{g}_{Na}/c$  is kept fixed to its original value of  $578 \text{ ms}^{-1}$ : the point  $(\hat{g}_L/c)_0 \approx 13 \text{ ms}^{-1}$  is a bifurcation point . Right: the plane  $(\hat{g}_{Na}/c, \hat{g}_L/c)$  and the boundary between the physiological and unphysiological regions.

**Figure 7** - The equilibria of the  $v$  variable as a function of  $\hat{g}_K/c$ , when  $\hat{g}_{Na}/c = 1064 \text{ ms}^{-1}$  and  $\hat{g}_L/c = 4.17 \text{ ms}^{-1}$  as in (7): the point  $(\hat{g}_K/c)_0 \approx 1840 \text{ ms}^{-1}$  is a bifurcation point.

**Figure 8** - A threshold simulation in the space-clamped 3-channels model with  $\hat{g}_K/c = 1850 \text{ ms}^{-1}$ : the system comes back to its resting state.

**Figure 9** - Threshold values for various pulse duration (circles: 'o') obtained with the 3-channels model ( $\hat{g}_K/c = 1850 \text{ ms}^{-1}$ ,  $L = 0.02 \text{ cm}$  and  $r = 0.4601 \text{ cm/ms}$ ). The continuous line shows Hill's interpolation (Mortimer, 1990) of these data, giving the strength-duration curve. The experimental data of Table I are also plotted (asterisks: '\*') for comparison purposes.



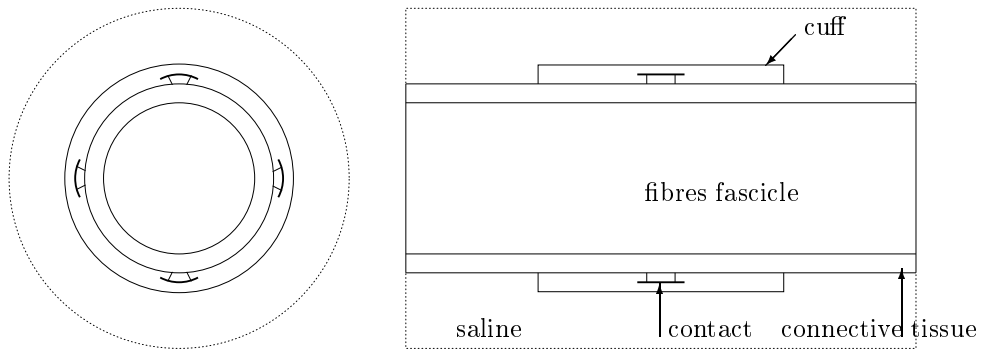


Figure 1: Transverse (left) and longitudinal (right) sections of the volume conductor domain and its subdomains. The drawing is not to scale. See text for geometrical and electrical parameters

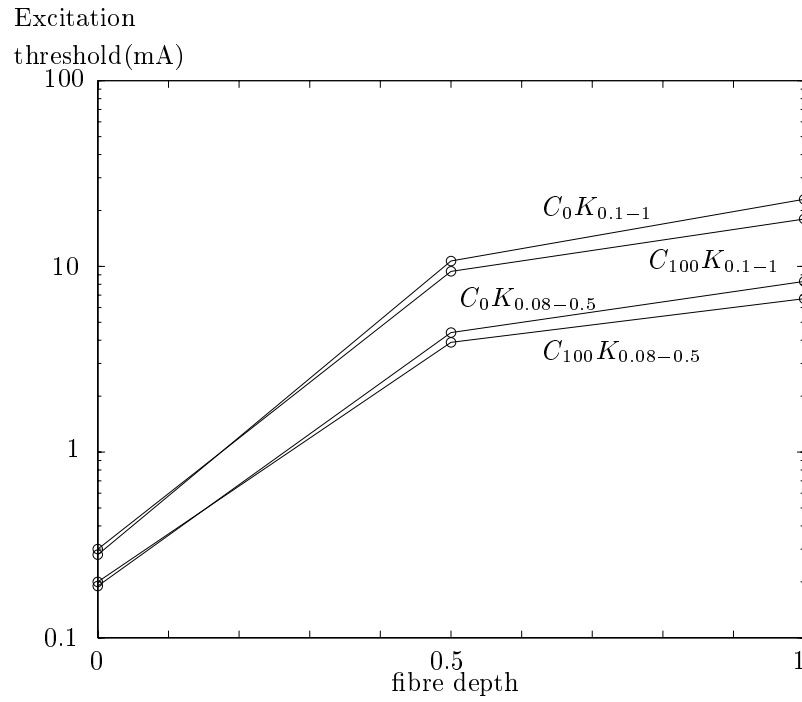


Figure 2: Effect of the volume conductor parameters (see Table II) on the fibre threshold. The CS model is adopted with  $L = 0.02 \text{ cm}$  and  $r = 0.5714 \text{ cm/ms}$ . The vertical axis is log-scaled. The fibre depth (horizontal axis) is defined as the distance of the fibre from the fascicle surface divided by the fascicle radius.

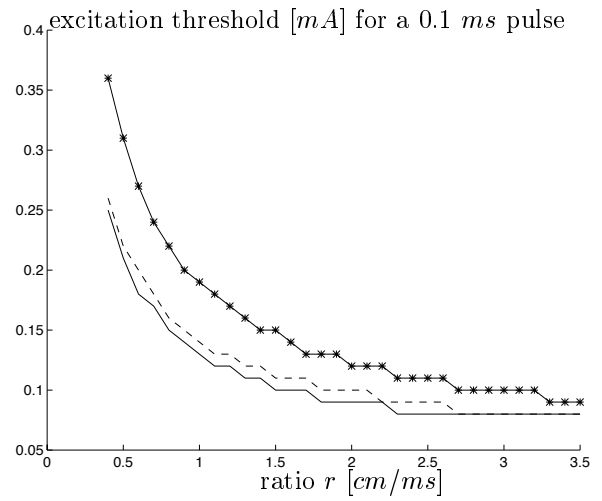
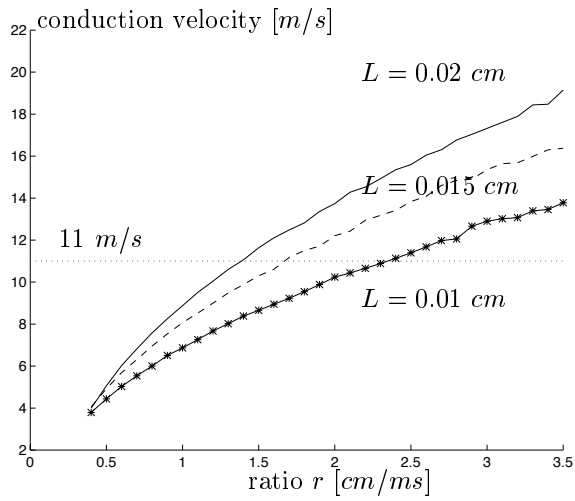


Figure 3: Effect of  $r$  and  $L$  on the conduction velocity and the excitation threshold. In the right graph, the same graphic conventions as in the left one are adopted for the  $L$  values.

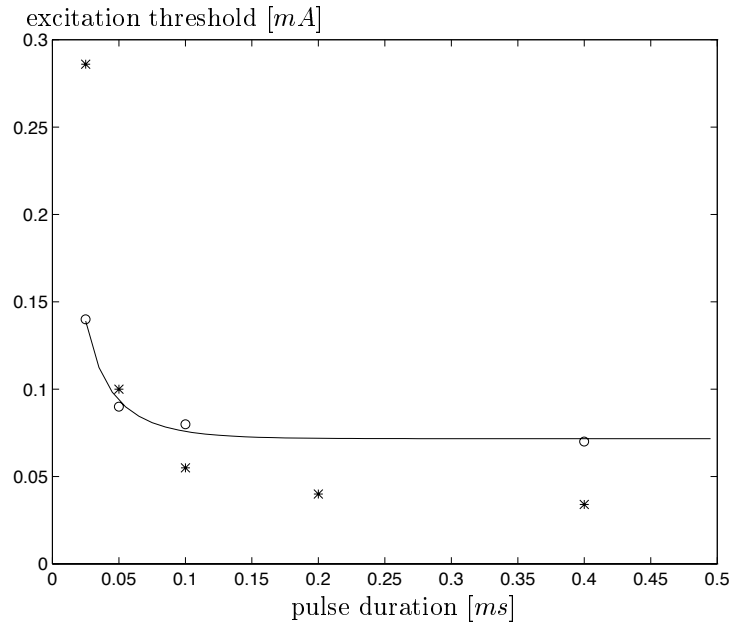


Figure 4: Threshold values for various pulse duration as predicted by the CS model (circles: 'o'), with  $r = 3 \text{ cm/ms}$  and  $L = 0.02 \text{ cm}$ . The continuous line shows Hill's interpolation (Mortimer, 1990) of these data, giving the strength-duration curve. The experimental data of Table I are also plotted (asterisks: '\*') for comparison purposes.

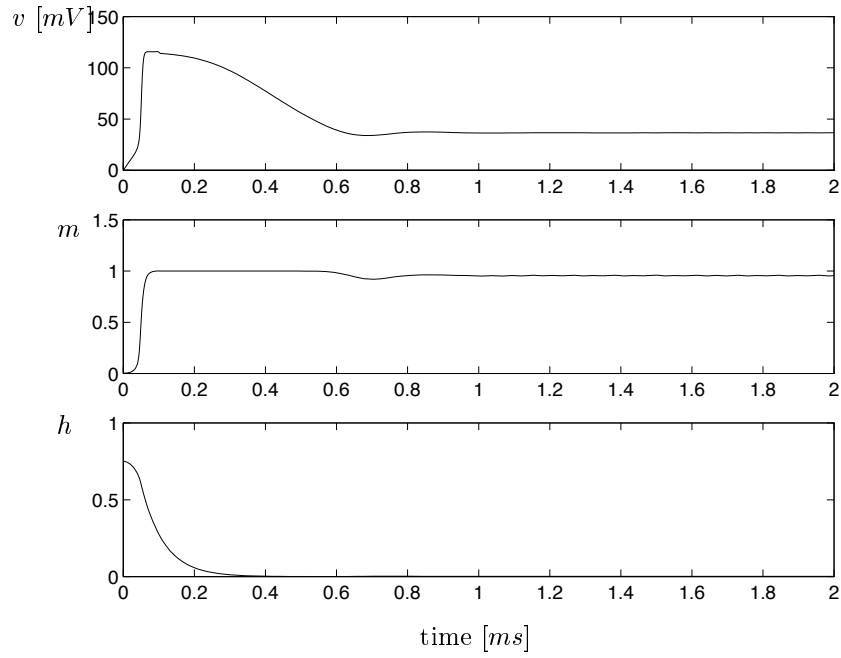


Figure 5: A threshold simulation in the 2-channels space-clamped system, when the ionic channel densities are set as in (7): a second equilibrium point ( $v_{eq} \approx 36$  mV,  $m_{eq} \approx 0.9$ ,  $h_{eq} \approx 0$ ) appears beside the resting state.

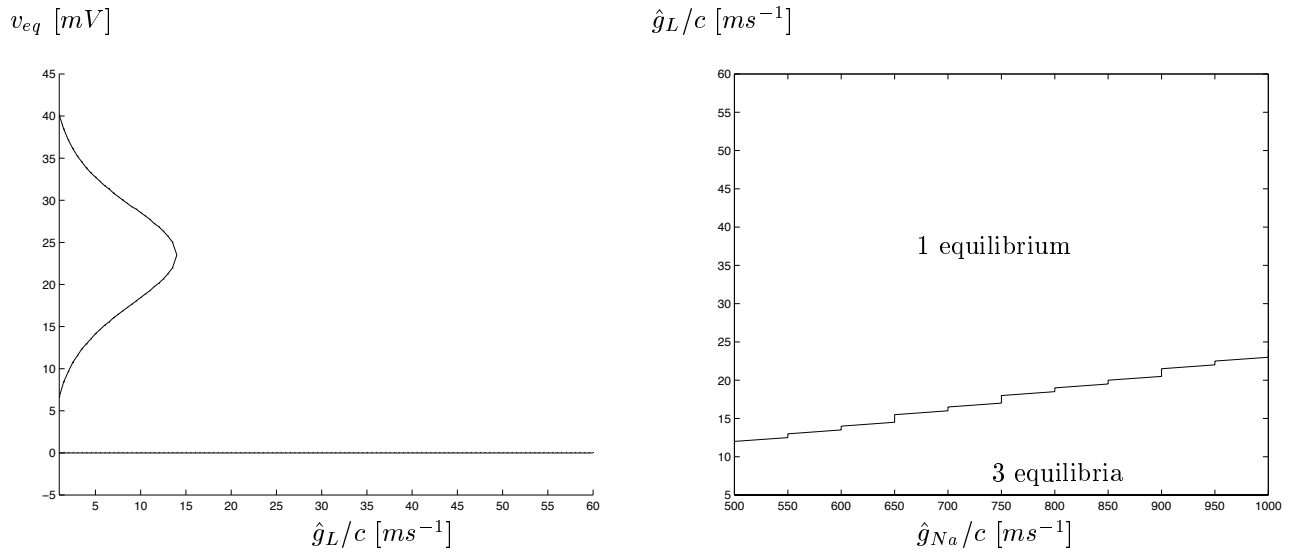


Figure 6: Left: the equilibria of the  $v$  variable as a function of  $\hat{g}_L/c$ , when  $\hat{g}_{Na}/c$  is kept fixed to its original value of  $578 \text{ ms}^{-1}$ : the point  $(\hat{g}_L/c)_0 \approx 13 \text{ ms}^{-1}$  is a bifurcation point. Right: the plane  $(\hat{g}_{Na}/c, \hat{g}_L/c)$  and the boundary between the physiological and unphysiological regions.

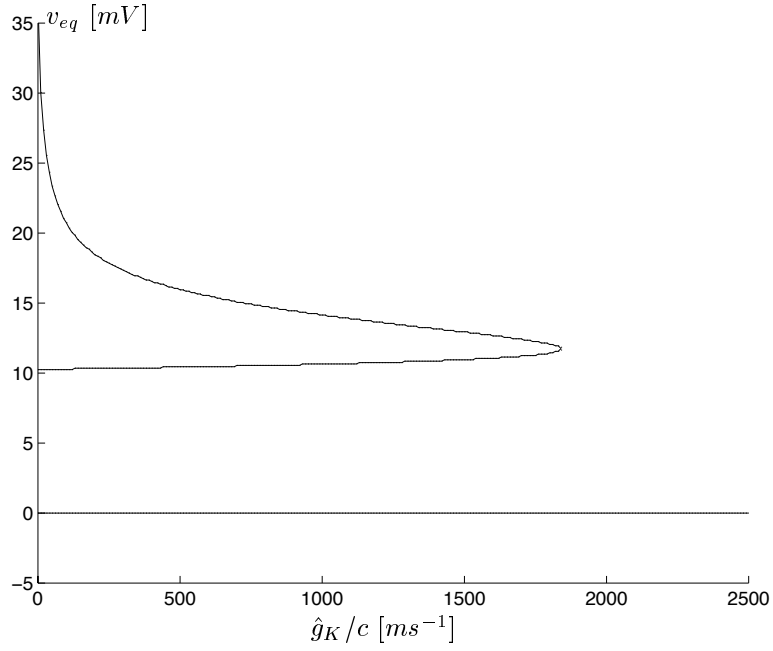


Figure 7: The equilibria of the  $v$  variable as a function of  $\hat{g}_K/c$ , when  $\hat{g}_{Na}/c = 1064 \text{ ms}^{-1}$  and  $\hat{g}_L/c = 4.17 \text{ ms}^{-1}$  as in (7): the point  $(\hat{g}_K/c)_0 \approx 1840 \text{ ms}^{-1}$  is a bifurcation point.

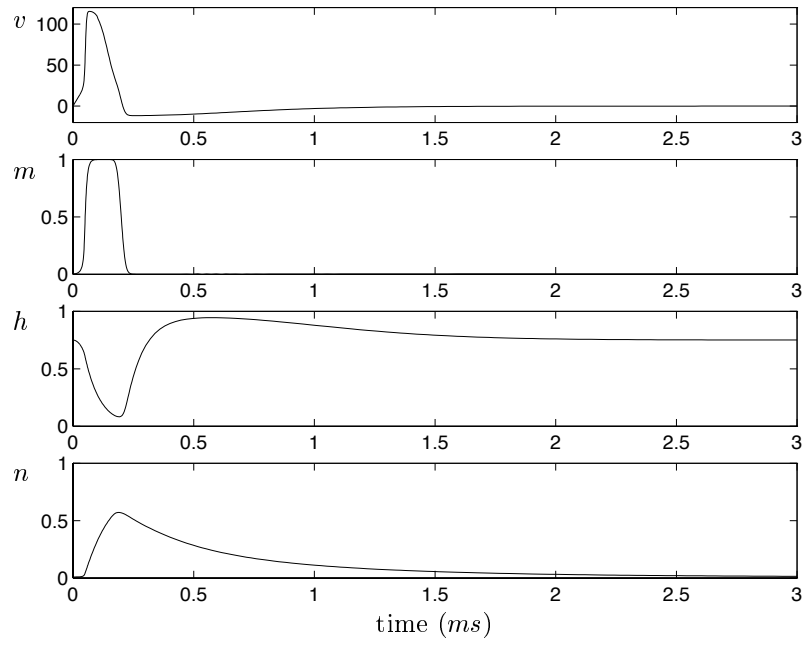


Figure 8: A threshold simulation in the space-clamped 3-channels model with  $\hat{g}_K/c = 1850 \text{ ms}^{-1}$ : the system comes back to its resting state.



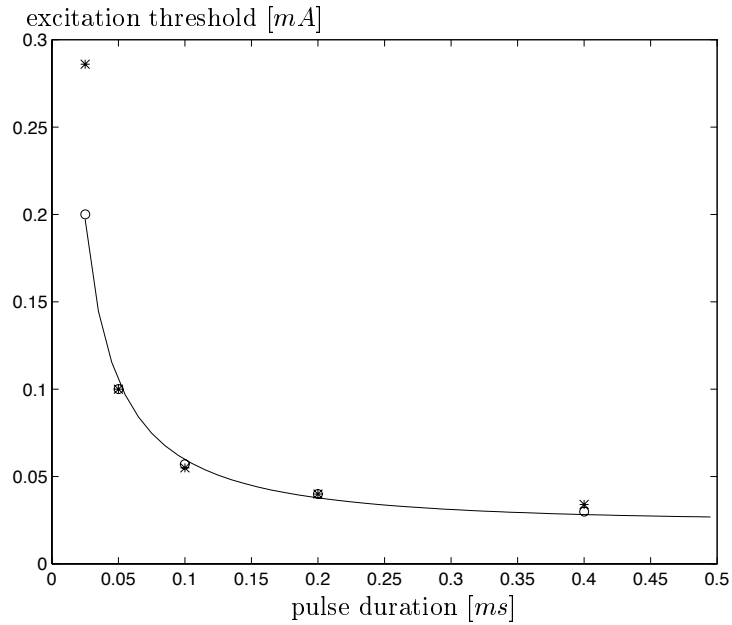


Figure 9: Threshold values for various pulse duration (circles: 'o') obtained with the 3-channels model ( $\hat{g}_K/c = 1850 \text{ ms}^{-1}$ ,  $L = 0.02 \text{ cm}$  and  $r = 0.4601 \text{ cm/ms}$ ). The continuous line shows Hill's interpolation (Mortimer, 1990) of these data, giving the strength-duration curve. The experimental data of Table I are also plotted (asterisks: '\*') for comparison purposes.